Electric field effect on electron spin splitting in SiGe/Si quantum wells

M. O. Nestoklon and E. L. Ivchenko
A.F. Ioffe Physico-Technical Institute, Russian Academy of Sciences, St. Petersburg 194021, Russia

J.-M. Jancu and P. Voisin
Laboratoire de Nanophotonique et Nanostructures, 91460 Marcoussis, France
(Received 11 January 2008; published 28 April 2008)

Effect of electric field on spin splitting in SiGe quantum wells (QWs) has been theoretically studied. Microscopic calculations of valley and spin splittings are performed in the efficient $sp^3d^5s^*$ tight-binding model. In accordance with the symmetry considerations, the electric field not only modifies the interface-induced spin splitting but also gives rise to a Rashba-type contribution to the effective two-dimensional electron Hamiltonian. Both the valley and spin splittings oscillate as a function of the QW width due to intervalley reflection of the electron wave off the interfaces. The oscillations of splitting are suppressed in rather low electric fields. The tight-binding calculations have been analyzed by using the generalized envelope-function approximation extended to asymmetrical QWs.

DOI: 10.1103/PhysRevB.77.155328 PACS number(s): 73.21.Fg, 71.70.Ej

I. INTRODUCTION

Understanding the details of semiconductor heterostructure electronic properties has been a key at each stage of their applications in the field of information and communication technologies. Presently, there is a broad interest in spin-dependent properties because they have a potential for novel "spintronic" devices, and beyond, because they govern for a large part the possible development of semiconductor-based quantum information processing. Spin splitting of electron dispersion relations arises from the combination of spin-orbit coupling and inversion asymmetry. Besides the contributions of bulk inversion asymmetry (BIA) first discussed by Dresselhaus in 1954 and the structure inversion asymmetry (SIA) introduced by Rashba and co-workers,[1,2] the existence of a contribution due to the breakdown of rotoinversion symmetry at an interface between two semiconductors was first suggested by Vervoort *et al.* in the late 1990s.[3,4] This "interface inversion asymmetry" (IIA) term was further documented both by group-theoretical analysis,[5] envelope-function calculations,[4] and measurements of circular polarization relaxation in quantum wells (QWs) based on various III-V semiconductors.[6–8] However, in these cases, the interface contribution appears in combination with BIA and SIA. Pure IIA can exist alone or together with SIA in heterostructures of centrosymmetric semiconductors such as Si-Ge QWs. Previous works[9] have established the symmetry properties specific to this system where electrons lie in states originating from the bulk X_z valleys. A general feature of zone-edge conduction valleys in bulk materials is their degeneracy (six for X valleys, four for L valleys) that gives rise to strong valley coupling when they are folded onto the two-dimensional Brillouin zone of a QW[10–15] or mixed in a zero-dimensional state in a Si quantum dot.[16] Valley coupling is another manifestation of the local, three-dimensional variations of crystal potential at semiconductor interfaces and quantitative estimates require atomistic information which is not available within the $\boldsymbol{k}\cdot\boldsymbol{p}$ theoretical framework. Parameters describing valley coupling must be extracted from microscopic approaches such as *ab initio* calculations or modeling using empirical parametrizations such atomistic pseudopotentials or tight-binding approach. The valley coupling strongly depends on the crystalline growth direction and shows an oscillating behavior as a function of the number of monolayers forming the X_z-valley or L-valley quantum well. It also depends on the overall symmetry of the quantum well, and for this reason, it can be modified by an external electric field. The spin splitting of in-plane dispersion relations in such systems results from the interplay of valley coupling and spin-dependent terms in the electron Hamiltonian. The case of L-valley QWs formed in the GaSb-AlSb system and grown along the [001] direction was first discussed in some details by Jancu *et al.*[12] In that case, the leading terms come from BIA invariants specific to the L valleys in combination with the L-valley coupling. For Si-Ge (001)-grown QWs, the interplay of IIA with X_z-valley coupling was examined from the $\boldsymbol{k}\cdot\boldsymbol{p}$ theory point of view and semiquantitative estimates were discussed in the frame of tight-binding calculations based on the sp^3s^* model.[11] However, it is well known that this simple model cannot quantitatively reproduce the properties of zone-edge valleys such as effective masses and dipole matrix element. This difficulty was solved in the late 1990s by the introduction of the extended basis $sp^3d^5s^*$ tight-binding model.[17] More recently, progress in the parametrization of this model has led to essentially perfect description of the electronic properties of bulk Ge (Ref. 18) and Si.[19] In this work, we use the advanced tight-binding model in combination with the envelope-function approach and calculate the conduction-band spin splitting that results from the interplay of valley coupling with the IIA and electric field effects in Si/SiGe quantum wells.

II. POINT-GROUP SYMMETRY ANALYSIS

In the virtual-crystal approximation for SiGe alloys, an ideal (001)-grown SiGe/Si/SiGe QW structure with an odd number N of Si-atomic planes has the point-group symmetry D_{2d} which allows the spin-dependent term $\alpha(\sigma_x k_x - \sigma_y k_y)$ in

the electron effective Hamiltonian, where σ_x, σ_y are the Pauli spin matrices, $\boldsymbol{k}$ is the two-dimensional wave vector with the in-plane components k_x, k_y, and $x\|[100]$, $y\|[010]$. Note that the invariant form of the pure IIA contribution is identical to that of the BIA or the Dresselhaus term in a QW; in this sense, IIA can be considered as a generalized Dresselhaus term. The QW structures with even N have the D_{2h} point symmetry containing the space-inversion center, the constant α is zero, and the two-dimensional electronic states are doubly degenerate. Under an electric field $\boldsymbol{F}=(0,0,F_z)$ applied along the growth direction z, the symmetry of QW structures with both odd and even numbers of Si monoatomic layers reduces to the C_{2v} point group and the spin-dependent linear-$\boldsymbol{k}$ Hamiltonian becomes

$$\mathcal{H}^{(1)}(\boldsymbol{k}) = \alpha(\sigma_x k_x - \sigma_y k_y) + \beta(\sigma_x k_y - \sigma_y k_x), \tag{1}$$

where the second contribution is the Rashba term (or the SIA term). In order to establish the parity of α, β with respect to inversion of the electric field, we note that, in the D_{2d} group, the combination $h(\boldsymbol{k})=\sigma_x k_x-\sigma_y k_y$ as well as even powers of F_z are invariants, while both the combination $h'(\boldsymbol{k})=\sigma_x k_y - \sigma_y k_x$ and odd powers of F_z transform according to the same representation B_2 (in notations of Ref. 20). Therefore, for structures with odd N, the coefficients α and β are, respectively, even and odd functions of F_z. They can be presented as

$$\alpha(F_z;\text{odd } N) = \alpha_0 + c_\alpha^{(2)} F_z^2 + c_\alpha^{(4)} F_z^4 + \cdots,$$

$$\beta(F_z;\text{odd } N) = c_\beta^{(1)} F_z + c_\beta^{(3)} F_z^3 + \cdots, \tag{2}$$

where $\alpha_0 \equiv \alpha(0)$ and $c_\alpha^{(2n)}$, $c_\beta^{(2n+1)}$ are field-independent coefficients. Similarly, for structures with even N, the linear-in-$\boldsymbol{k}$ spin-dependent Hamiltonian can be presented in the form

$$\mathcal{H}^{(1)}(F_z;\text{even } N) = F_z[C_1 h(\boldsymbol{k}) + C_2 h'(\boldsymbol{k})], \tag{3}$$

where C_1, C_2 are even functions of F_z. The above representation immediately follows if we take into account that, with respect to operations of the D_{2h} group, both $h(\boldsymbol{k})$ and $h'(\mathbf{k})$ transform in the same way as the component F_z does.

The aim of this work is to calculate and analyze the electric field dependencies of α and β. For this purpose, we use the precise nearest-neighbor $sp^3d^5s^*$ tight-binding model[17] and calculate valley and spin splittings in symmetrical QWs in the absence and presence of an external electric field.

III. TIGHT-BINDING MODEL

To calculate electron subband splittings, we use the $sp^3d^5s^*$ tight-binding theory elaborated by Jancu *et al.*[17] It perfectly reproduces band structure of indirect bulk semiconductors, as well as electron effective masses, etc. In particular, the parametrization used in this work reproduces the value $k_0=85\%$ of the conduction-band minimum in Si, which was considered as a challenge.[21] Moreover, it is demonstrated[22] that the resulting spin splittings in conduction band of semiconductors are well described in the whole Brillouin zone. One of the main advantages of this method is a very straightforward treatment of nanostructures.

In Ref. 11, we estimated the electron spin splitting in symmetrical SiGe QWs by using a less detailed sp^3s^* tight-binding model, which allowed us to understand the main qualitative features of spin splitting as well as to demonstrate the observability of this effect in Si/SiGe heterostructures.

In the tight-binding model, the electron wave function is written as a linear combination of atomic orbitals,[23]

$$|\psi,\boldsymbol{r}\rangle = \sum_{n,\nu} C_{n,\nu} |\Psi_\nu, \boldsymbol{r}-\boldsymbol{r}_n\rangle, \tag{4}$$

where n enumerates the atoms in the structure and ν runs through the set of spinor orbitals at the nth atom. In the $sp^3d^5s^*$ model, this set includes the orbitals s, p_η ($\eta=x,y,z$), d_ξ ($\xi=yz$, xz, yz, x^2-y^2, $2z^2-x^2-y^2$), and s^* multiplied by the spinors $\uparrow$ and $\downarrow$. We assume the basic orbital functions to be orthogonal.[24] Thus, the tight-binding Hamiltonian is presented as a multicomponent matrix and the Schrödinger equation as an eigenvalue problem,

$$\sum_{n',\nu'} \langle \Psi_{n,\nu}|H|\Psi_{n',\nu'}\rangle C_{n',\nu'} = E C_{n,\nu}, \tag{5}$$

where $|\Psi_{n,\nu}\rangle = |\Psi_\nu, \boldsymbol{r}-\boldsymbol{r}_n\rangle$. The Hamiltonian matrix elements depend on the relative position of atoms, $\boldsymbol{r}_n-\boldsymbol{r}_{n'}$, and chemical type of atoms n and n'. We use here the nearest-neighbor approximation where the matrix elements differ from zero only for neighboring atoms. The detailed procedure of constructing the tight-binding Hamiltonian can be found in Ref. 23. Strain effects can be included by scaling the matrix elements with respect to the bond-angle distortions and bond-length changes.[25]

For the SiGe alloy, we use the virtual-crystal approximation in order to concentrate on the intrinsic structure symmetry. Thus, we neglect all the effects of disorder. Tight-binding parameters were optimized to carefully reproduce alloy band structure. The strain in the relaxed structure is treated into two ways. First, atomic positions used in calculations are chosen by using Van de Walle's model.[26] We have also applied Keating's valence force field model[27] with the SiGe parameters from Ref. 28 and found no difference between the continuous and atomistic approaches.

In addition to the strain dependence of tight-binding parameters, we have modified the structure potential (see below) with respect to experimentally observed $Si/Si_{1-x}Ge_x$ conduction-band offset.[29,30] The valence band offset is not derived from the present calculation; it is introduced as an additional model parameter, which characterizes the interface. This approach was found to give an excellent description of the band structure of ultrashort period Si/Ge superlattice in complete agreement with *ab initio* calculations.[31]

We treat an electric field in the tight-binding approach in the following way:[32] the diagonal matrix elements of the tight-binding Hamiltonian are shifted due to the potential of the applied electric field,

$$\langle \Psi_{n,\nu}|H|\Psi_{n',\nu'}\rangle = \langle \Psi_{n,\nu}|H|\Psi_{n',\nu'}\rangle_{U=0} + U(\boldsymbol{r}_n)\delta_{nn'}\delta_{\nu\nu'}, \tag{6}$$

where $U(\boldsymbol{r})$ is the electric potential energy.

Since we are interested in the in-plane dispersion of free electrons in a heterostructure, we impose periodical boundary conditions in the interface plane (001). Because of the periodicity in the [100] and [010] directions, we can introduce the in-plane wave vector $\boldsymbol{k}$ and, for a given value of $\boldsymbol{k}$, construct the tight-binding Hamiltonian with a discrete spectrum. For the sake of numerical simplicity, we also use periodic boundary conditions along the growth direction [001] taking the barrier layers thick enough to exclude the influence of their thickness on the calculated values of α and β. It follows immediately from the band structure of silicon and SiGe/Si/SiGe structure potential that, neglecting the valley splitting, the electronic states with $k_x=k_y=0$ are fourfold degenerate. We focus on the dispersion of the lowest conduction subband $e1$. The interface-induced valley mixing leads to a splitting of the state $|e1,\boldsymbol{k}=0\rangle$ into two spin-degenerate states denoted (+) (upper subband) and (−) (lower subband). At nonzero $\boldsymbol{k}$, each subband, (+) and (−), undergoes the spin-orbit splitting described by Eq. (1) with the coefficients $\alpha_\pm$ and $\beta_\pm$ for the valley-orbit split subbands ($\pm$). It is instructive to rewrite Eq. (1) in the coordinate frame $x' \| [1\bar{1}0]$, $y' \| [110]$ as follows:

$$\mathcal{H}^{(1)}(\boldsymbol{k}) = (\alpha_\pm + \beta_\pm)\sigma_{x'}k_{y'} + (\alpha_\pm - \beta_\pm)\sigma_{y'}k_{x'}. \qquad (7)$$

Let us introduce the energy difference $\Delta_{so}^{(\pm)}(\boldsymbol{k}\|[1\bar{1}0])$ for the states $|\pm,\boldsymbol{k}\|[1\bar{1}0]\rangle$ with the spin polarized parallel and antiparallel to [110] and $\Delta_{so}^{(\pm)}(\boldsymbol{k}\|[110])$ for the states $|\pm,\boldsymbol{k}\|[110]\rangle$ with the spin polarized parallel and antiparallel to $[1\bar{1}0]$. The modulus of $\Delta_{so}^{(\pm)}(\boldsymbol{k})$ gives the spin splitting of the $\pm$ subbands and the sign of $\Delta_{so}^{(\pm)}(\boldsymbol{k})$ determines the relative position of the split spin sublevels. It follows from Eq. (7) and the definition of $\Delta_{so}^{(\pm)}(\boldsymbol{k})$ that the constants $\alpha_\pm$, $\beta_\pm$ can be found from

$$\alpha_\pm = \lim_{k\to+0} \frac{\Delta_{so}^{(\pm)}(\boldsymbol{k}\|[110]) + \Delta_{so}^{(\pm)}(\boldsymbol{k}\|[1\bar{1}0])}{4|\boldsymbol{k}|},$$

$$\beta_\pm = \lim_{k\to+0} \frac{\Delta_{so}^{(\pm)}(\boldsymbol{k}\|[110]) - \Delta_{so}^{(\pm)}(\boldsymbol{k}\|[1\bar{1}0])}{4|\boldsymbol{k}|}. \qquad (8)$$

Also, it should be pointed out that, since the studied QWs are quite shallow, the electron dispersion should be treated with care. To avoid nonlinear effects, very small values of k_x, k_y should be considered.

IV. RESULTS AND DISCUSSION

A. Numerical $sp^3d^5s^*$ model calculations: Unbiased structure

In order to test and improve our previous results, we calculated valley and spin splitting in symmetrical Si QW with $Si_{0.75}Ge_{0.25}$ barriers as a function of the QW width. For SiGe composition, we used optimized tight-binding parameters precisely reproducing realistic alloy band structure. The strategy for parametrization of the Ge-Si alloy in a virtual-crystal approximation is as follows: the parameters of Ge and Si hydrostatically strained to the alloy parameter are first calculated and linearly interpolated. The small remaining differences with measured values are then corrected by fine tuning of a few two-center parameters. For interface atoms, we use linear combination of pure Si parameters and alloy.

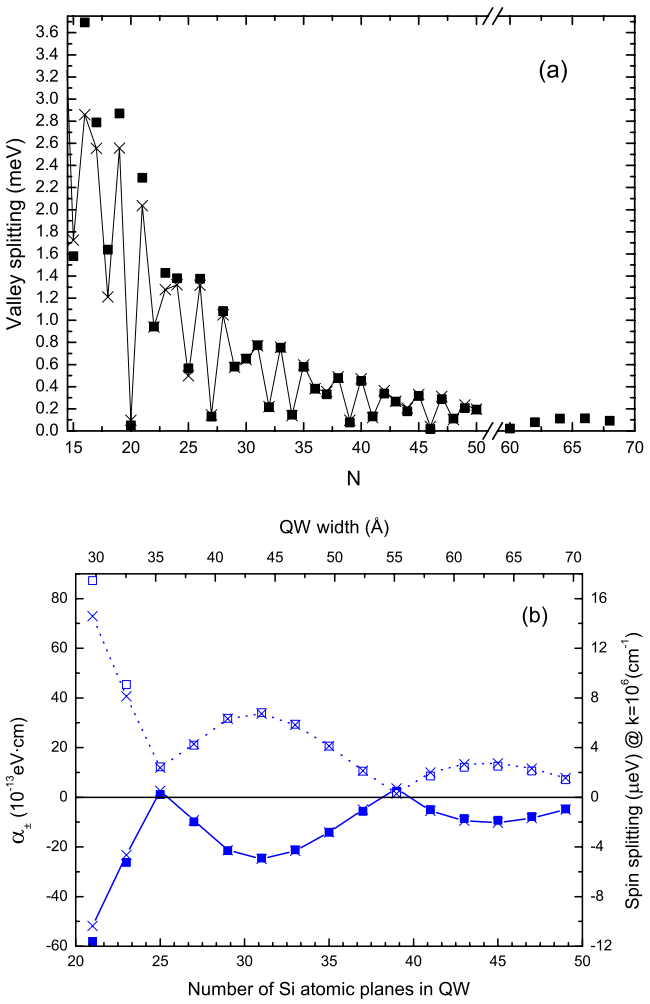

FIG. 1. (Color online) (a) Valley splitting Δ_v as a function of N in a $Si_{1-x}Ge_x/Si/Si_{1-x}Ge_x$ (x=0.25) QW structure in the absence of an electric field. Solid squares and vortices of the broken line represent the results of calculations by using the tight-binding method and envelope-function approximation, respectively. (b) Spin-splitting constants $\alpha_\pm$ versus the number N of Si monoatomic layers in the same system (odd N are taken in account only). Spin splitting is shown by solid and open squares ($sp^3d^5s^*$ tight-binding calculation, α_- and α_+, respectively) and X-shaped crosses (envelope-function approximation).

Tight-binding parameters are optimized for bulk materials. However, band offsets at the interfaces in the heterostructure are also important. For conduction-band offset, we use Shäffler's paper[30] as a reference. Thus, we take a value of 150 meV as a conduction-band offset for X_z-valley electrons.

Figure 1 shows the zero-field results of calculation of (a) the valley splitting Δ_v and (b) the constants $\alpha_\pm$ for the valley-split $e1$ subbands in a symmetrical single QW structure with odd-N Si-atomic planes sandwiched between the thick $Si_{0.75}Ge_{0.25}$ barriers. The splittings as a function of N exhibit oscillations, in agreement with Refs. 10–15. In Fig. 1, X-shaped crosses depicted as vortices of the broken line rep-

resent the calculation in the envelope-function approximation (see below). The broken line is drawn to guide the eyes. Note that, in order to simplify comparison with the results obtained by other authors, Fig. 1(a) illustrates the valley splitting not only for the QW width region of 15–50 Å but also for the region of 60–70 Å.

The results obtained in the framework of the advanced $sp^3d^5s^*$ tight-binding model show considerable difference with our previous estimates.[11] The valley splitting is significantly smaller; its value decreases by a factor of 3, whereas the spin splitting increases almost six times (see below). This difference is not unexpected since a careful tight-binding treatment of Si and its compounds is possible in the $sp^3d^5s^*$ model only.

The previous theoretical values for valley splitting were obtained by both tight-binding[10,15] and pseudopotential methods.[13] Although the first two papers utilize the method of calculation similar to that applied here, a straightforward comparison is not possible due to different parametrizations of the $Si_{1-x}Ge_x$ alloy as well as different alloy compositions (x=0.2 in Ref. 10 and 0.3 in Ref. 15) and conduction-band offsets used. However, our results are in good agreement with the both estimates. For example, for a QW containing 64 Si-atomic layers (32 monomolecular layers, 9 nm), we obtain for the valley splitting an ~0.11 meV, while Refs. 10 and 15 present the coinciding values of ~0.2 meV. Our analysis shows that the valley splitting is quite sensitive to the SiGe alloy parameters. By using the linear combination of Si and Ge tight-binding parameters for the alloy, we could reproduce the values of the valley splitting obtained by Boykin *et al.*[10]

Comparison with Ref. 13 is more straightforward. Figure 1 in the cited paper shows dependence of the valley splitting on the barrier Ge content for a 16 Si-atomic layer QW calculated by the empirical pseudopotential method. In particular, for the $Si_{0.75}Ge_{0.25}/Si/Si_{0.75}Ge_{0.25}$ QW, the valley splitting of about 2.5 meV was obtained,[13] while our estimate is 3.7 meV. This is in a good agreement taking into account that the two values are obtained in two completely different approaches for quite narrow QWs where interface effects are extremely important.

Figure 2 shows the valley and spin-splitting constants as a function of the conduction-band offset for QWs with 31, 32, 33, 34, and 64 Si-atomic layers. The fifth structure is taken in order to provide comparison with Refs. 10 and 15. In Fig. 2, in addition to the tight-binding calculations, we present analytical results on valley and spin splittings in the framework of the extended envelope-function approach. A detailed discussion of the analytical treatment is given in Sec. IV C. Here, we only point out an excellent agreement between the results for the splittings as a function of the QW width and satisfactory description of the dependence of these splittings on the band offset.

B. Numerical calculations in the presence of electric field

Figure 3 demonstrates the variation of spin-splitting constants with the electric field F_z for the $e1$ valley-split subbands. In accordance with symmetry considerations, the calculations show that the spin splitting becomes anisotropic in QWs with odd numbers of atomic planes and appears in QWs with even numbers of atomic planes. The variation of valley splitting is very weak and we do not present it here.

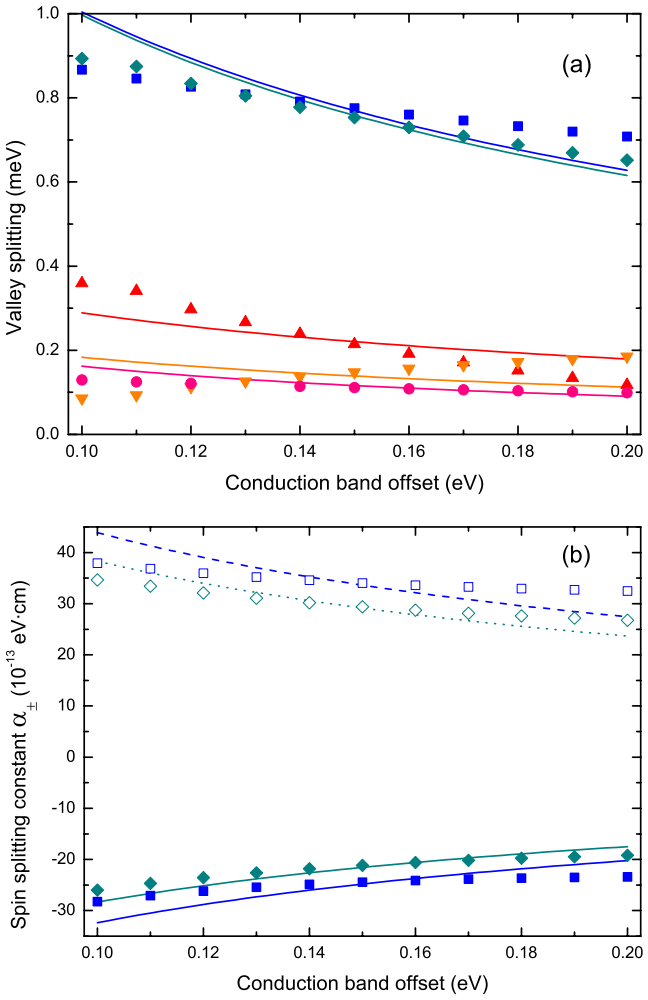

FIG. 2. (Color online) (a) Valley and (b) spin splittings for the lowest conduction subband versus the conduction band offset. (a) The valley splitting calculated for five QWs with N=31(■), 32(▲), 33(♦), 34(▼), and 64(●) Si monoatomic planes. (b) The spin-splitting constants α_- (■,♦) and α_+ (□,◇) for 31 (■,□) and 33(♦,◇) Si-atomic layers. The fitting by using the extended envelope-function approach is shown by corresponding lines.

To determine the coefficients $\alpha_\pm$ and $\beta_\pm$, we performed the tight-binding calculation of the spin splittings for the electron wave vectors $\boldsymbol{k}\|[110]$ and $\boldsymbol{k}\|[1\bar{1}0]$ and then applied Eqs. (8) to directly find the constants α and β. The electric field is introduced as a shift of diagonal energies in the tight-binding Hamiltonian. In accordance with Eq. (6), we choose electrostatic potential to be a linear function of z both inside the QW and in the barrier areas near the interfaces. The area of the constant electric field is extended deep into barriers in order to neglect dependence of the splitting on the choice of potential profile. Note that the field values in Fig. 3 are small enough to avoid the tunneling of an electron from the QW into the barriers.

At zero electric field, β=0 for arbitrary value of N and, similarly, α=0 for even N. In this case, the spin splitting

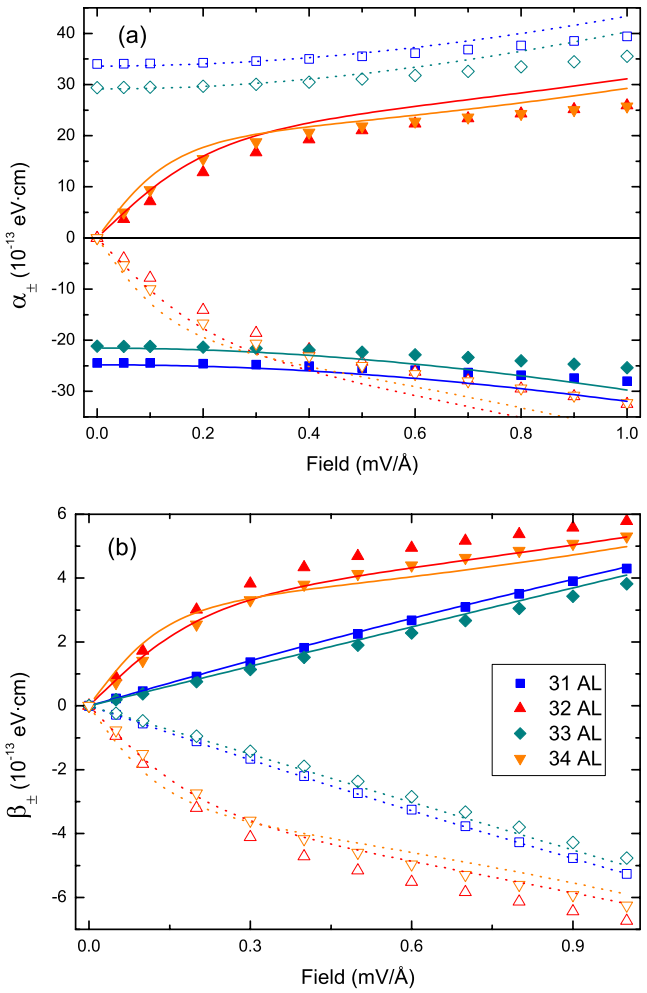

FIG. 3. (Color online) Spin-splitting constants $\alpha_\pm$ and $\beta_\pm$ for the lowest conduction subband versus the electric field F_z calculated for four QWs with 31, 32, 33, and 34 Si monoatomic planes. Points are calculated in the $sp^3d^5s^*$ tight-binding model. Lines represent fitting by using the extended envelope-function approach.

$\Delta_{so}(\boldsymbol{k})$ is independent of the azimuthal angle of the $\boldsymbol{k}$ vector. However, with increasing the field, the diversity in values of α and β for QWs with $N=31$, 32, 33, and 34 decreases.

The further discussion of spin splitting as a function of electric field is continued in the next section. It suffices to note here that for the low fields, the coefficients $\alpha_\pm$ in QWs with odd N are linear functions of F_z^2. In contrast, in QWs with even numbers of atomic planes where the spin splitting is absent at zero field, $\alpha_\pm$ are proportional to F_z. We stress that the field-induced change of $\alpha_\pm$ (odd N) becomes comparable to the zero-field value of $\alpha_\pm$ in quite weak fields $F_z \sim 4\times 10^4$ V/cm.

In the previous paper,[11] we developed the extended envelope-function model in order to demonstrate that the spin splitting in macroscopically symmetrical QWs is fully defined by interfaces. At nonzero electric field, two mechanisms are possible, namely, the SIA and IIA mechanisms. One of the goals of current research is to establish the most important term in realistic QWs. To reveal carefully the comparative role of two mechanisms, we present analytical treatment of results shown in Figs. 2 and 3 in the framework of the envelope-function approach.

C. Extended envelope-function approach

Here, we propose an extended envelope-function approach[11] to describe the valley and spin splittings in the presence of an external or built-in electric field. The electron wave function is written as

$$\Psi(\boldsymbol{r}) = e^{i\boldsymbol{k}_\parallel\cdot\boldsymbol{\rho}}[\varphi_1(z)\psi_{\boldsymbol{k}_0}(\boldsymbol{r}) + \varphi_2(z)\psi_{-\boldsymbol{k}_0}(\boldsymbol{r})], \tag{9}$$

where $\psi_{\pm\boldsymbol{k}_0}(\boldsymbol{r}) = e^{\pm ik_0 z}u_{\pm\boldsymbol{k}_0}(\boldsymbol{r})$ is the Bloch function at the extremum points $\pm\boldsymbol{k}_0$ on the line Δ in the Brillouin zone. The spinor envelopes φ_1, φ_2 in Eq. (9) are conveniently presented as a four-component bispinor,

$$\hat{\varphi}(z) = \begin{bmatrix} \varphi_1(z) \\ \varphi_2(z) \end{bmatrix}. \tag{10}$$

The effective Hamiltonian acting on $\hat{\varphi}(z)$ is written as a 4×4 matrix consisting of the standard zero-approximation Hamiltonian,

$$\mathcal{H}_0 = \frac{\hbar^2}{2}\left[-\frac{d}{dz}\frac{1}{m_l(z)}\frac{d}{dz} + \frac{k_x^2+k_y^2}{m_t(z)} + U(z)\right], \tag{11}$$

which is independent of valley and spin indices, and an interface-induced δ-functional perturbation,

$$\mathcal{H}' = \hat{V}_L\delta(z-z_L) + \hat{V}_R\delta(z-z_R). \tag{12}$$

Here, m_l and m_t are the longitudinal and transverse electron effective masses in the Δ valley of the bulk material, z_L and z_R are the coordinates of the left- and right-hand-side interfaces, the potential energy $U(z)$ is referred to the bottom of the conduction band in Si and given by

$$U(z) = V\theta_b(z) - eF_z z,$$

with V being the conduction-band offset, $\theta_b(z)=1$ in the SiGe barrier layers, and $\theta_b(z)=0$ inside the Si layer. The explicit form of the matrices $\hat{V}_{L,R}$ obtained by using symmetry considerations is presented in Ref. 11.

In the zero approximation, i.e., neglecting the valley-orbit and spin-orbit couplings, $\hat{V}_{L,R}=0$, the bispinor is given by

$$\hat{\varphi}(z) = \begin{bmatrix} c_1 \\ c_2 \end{bmatrix}\chi(z),$$

where c_1, c_2 are arbitrary z-independent spinors and the function $\chi(z)$ satisfies the Schrödinger equation,

$$\mathcal{H}_0\chi(z) = E\chi(z). \tag{13}$$

In the following, we take into consideration only the lowest size-quantized electronic subband $e1$.

The next step is an allowance for the interface-induced spin-independent mixing between the valleys $\boldsymbol{k}_0$ and $-\boldsymbol{k}_0$ described by the matrices,

$$\hat{V}_R = \begin{bmatrix} 0 & \Lambda_R \\ \Lambda_R^* & 0 \end{bmatrix}, \quad \hat{V}_L = \begin{bmatrix} 0 & \Lambda_L \\ \Lambda_L^* & 0 \end{bmatrix},$$

where $\Lambda_R = \lambda e^{-ik_0 a}$, $\Lambda_L = \lambda^* e^{ik_0 a}$, $a = z_R - z_L = Na_0/4$ is the QW width, a_0 is the microscopic lattice constant, and λ is a complex coefficient.

In terms of the envelope $\chi(z)$, the matrix element of valley mixing can be written as

$$\langle 1|\mathcal{H}'|2\rangle = |\lambda|[(\chi_L^2 + \chi_R^2)\cos(k_0 a - \phi_\lambda) + i(\chi_L^2 - \chi_R^2) \times \sin(k_0 a - \phi_\lambda)], \tag{14}$$

where $|\lambda|$ and ϕ_λ are the modulus and the phase of λ, $\chi_{R,L}$ are the values of the envelope χ at the right and left interfaces, $\chi(\pm a/2)$, respectively. The valley-orbit split states have the energy $E_\pm = E_0 \pm |\langle 1|\mathcal{H}'|2\rangle|$, where E_0 is the eigenenergy of Eq. (13), so that the splitting is equal to

$$\Delta_v = 2|\langle 1|\mathcal{H}'|2\rangle| = 2|\lambda|\sqrt{\chi_L^4 + \chi_R^4 + 2\chi_L^2\chi_R^2\cos[2(k_0 a - \phi_\lambda)]}. \tag{15}$$

The bispinors for the upper (+) and lower (−) states are given by

$$\hat{\varphi}_{\pm,s}(z) = \frac{1}{\sqrt{2}}\begin{bmatrix} c_s \\ \pm e^{-i\phi_M} c_s \end{bmatrix}, \tag{16}$$

where c_s is the spinor $\uparrow$ for the electron spin $s = 1/2$ and $\downarrow$ for the electron spin $s = -1/2$, ϕ_M is the phase of matrix element (14).

The tight-binding calculations show that the spin splitting is much smaller as compared to the valley splitting Δ_v. Therefore, the spin splitting can be independently considered for the upper and lower valley-orbit split states [Eq. (16)]. The corresponding matrix elements are reduced to

$$\mathcal{H}'_{ss'}(\boldsymbol{k}; e1, \pm) = M_{1s,1s'} \pm (\mathrm{Re}\{M_{1s,2s'}\}\cos\phi_M + \mathrm{Im}\{M_{1s,2s'}\}\sin\phi_M), \tag{17}$$

where the subscript indices 1, 2 enumerate the valleys $\boldsymbol{k}_0$, $-\boldsymbol{k}_0$ and s, $s' = \pm 1/2$ are the spin indices, the components $M_{1s,1s'}$, $M_{1s,2s'}$ written as 2×2 matrices M_{11}, M_{12} are related to the similar 2×2 matrices $V_{R,11}$, $V_{L,11}$, $V_{R,12}$, $V_{L,12}$ by

$$M_{11} = \chi_L^2 V_{L,11} + \chi_R^2 V_{R,11}, \quad M_{12} = \chi_L^2 V_{L,12} + \chi_R^2 V_{R,12}.$$

The spin-dependent contributions to $V_{R,11}$, $V_{L,11}$, $V_{R,12}$, and $V_{L,12}$ are linear combinations of $h(\boldsymbol{k})$ and $h'(\boldsymbol{k})$ (see Ref. 11),

$$\hat{V}_R = \begin{bmatrix} Sh(\boldsymbol{k}) + S'h'(\boldsymbol{k}) & [\lambda + ph(\boldsymbol{k}) + p'h'(\boldsymbol{k})]e^{-ik_0 a} \\ [\lambda^* + p^* h(\boldsymbol{k}) + p'^* h'(\boldsymbol{k})]e^{ik_0 a} & Sh(\boldsymbol{k}) + S'h'(\boldsymbol{k}) \end{bmatrix}, \tag{18}$$

and similar equation for $\hat{V}_L$ with the coefficients interrelated to λ, S, S', p, p' due to the mirror-rotation operation $\mathcal{S}_4$ (odd N) or the inversion i (even N) which transforms the right-hand-side interface into the left-hand-side one. Taking into account the relation between coefficients entering the matrices $\hat{V}_R$ and $\hat{V}_L$ and the notations of Ref. 11, we can write the spin Hamiltonians (17) in the form of Eq. (1), namely,

$$\mathcal{H}^{(1)}(\boldsymbol{k}; e1, \pm) = \alpha_\pm h(\boldsymbol{k}) + \beta_\pm h'(\boldsymbol{k}). \tag{19}$$

For the coefficients $\alpha_\pm$, $\beta_\pm$ describing the spin splitting of the valley-orbit split subbands, we obtain

$$\alpha_\pm = [\chi_R^2 - (-1)^N \chi_L^2]S \pm |p| H_\alpha(\phi_p),$$

$$\beta_\pm = (\chi_R^2 - \chi_L^2)S' \mp |p'| H_\beta(\phi_{p'}). \tag{20}$$

Here,

$$H_\alpha(\phi) = \chi_R^2 \cos(k_0 a - \phi + \Phi) - (-1)^N \chi_L^2 \cos(k_0 a - \phi - \Phi),$$

$$H_\beta(\phi) = \chi_R^2 \cos(k_0 a - \phi + \Phi) - \chi_L^2 \cos(k_0 a - \phi - \Phi),$$

$$\Phi = \arg(\chi_L^2 e^{i(k_0 a - \phi_\lambda)} + \chi_R^2 e^{-i(k_0 a - \phi_\lambda)}),$$

the parameters S, S' describe the intravalley contributions to the interface-induced electron spin mixing, and the parameters $p = |p|e^{i\phi_p}$ and $p' = |p'|e^{i\phi_{p'}}$ describe the spin-dependent intervalley mixing. Oscillatory dependence of the valley and spin splittings on the QW thickness a is caused by interference of electron waves arising from intervalley reflection off the left- and right-hand-side interfaces.

D. Comparison between tight-binding and envelope-function approach

In the absence of an electric field, one has $\chi_L^2 = \chi_R^2$, with $\Phi = 0$ for positive and $\Phi = \pi$ for negative values of $\cos(k_0 a - \phi_\lambda)$, and Eqs. (15) and (20) reduce to[11]

$$\Delta_v = 4\chi_L^2 |\lambda \cos(k_0 a - \phi_\lambda)|,$$

with $\alpha_\pm = \beta_\pm = 0$ for even N, and

$$\alpha_\pm = 2\chi_L^2[S \pm \eta|p|\cos(k_0 a - \phi_p)], \quad \beta_\pm = 0,$$

for odd N, where $\eta = e^{i\Phi} = \mathrm{sgn}\{\cos(k_0 a - \phi_\lambda)\}$. The curves in Fig. 1 are calculated by using the following best-fit set of parameters: $|\lambda| = 65$ meV Å, $\phi_\lambda = 0.013\pi$, $|p| = 4450$ meV Å^2, $\phi_p = 0.095\pi$, and $S = 650$ meV Å^2.

Although tight-binding-model values of the coefficients in the present work are quite different from the previous estimates, the envelope-function approach proves its adequate description of the valley and spin splittings as a function of

the QW width. The analytical approach with merely five parameters perfectly fits the complex microscopic calculation.

Comparison of new results with the experimental data of Wilamovsky *et al.*[33] shows the better agreement. With the necessary correction,[34] the experimental results give $\sim 3.4 \times 10^{-13}$ eV Å for the spin-splitting constant α_- in a 120-Å-thick QW. The tight-binding calculation in a structure with 85 atomic layers of Si gives $\alpha_- = 2.1 \times 10^{-13}$ eV Å without electric field. Under applied electric field of 0.3 V Å, we have obtained $\alpha_- = 4.1 \times 10^{-13}$ eV Å and $\beta_- = 1.1 \times 10^{-13}$ eV Å. The more detailed comparison should be done with caution since effects of disorder and built-in electric fields may have crucial influence. However, the coincidence in an order of magnitude shows that our calculations agree with the available experimental data.

According to Fig. 2, the description of dependence of spin splitting on the band offset is not so perfect in the framework of envelope-function approach. In fact, the variation in band offset results in a complex (obviously nonlinear) behavior of the parameters in the boundary conditions at the interfaces.

Figure 3 is the main result of this work and we discuss it in more details. The agreement between the two approaches seen in Fig. 3(a) shows that the extended envelope-function approach catches the physics of spin splitting induced by the applied electric field. Moreover, the fact that this agreement takes place with no addition of a SIA term to Eqs. (20) shows that in the system under study, the IIA contribution is dominating by more than an order of magnitude. This result is in line with the calculation of spin splitting of conduction subbands in III-V heterostructures where the contribution proportional to the average value of the electric field amounts only a few percent of the interface contribution.[35] It should be noted that Eqs. (20) for $\alpha_\pm$ contains only parameters which can be extracted from Fig. 1, and, indeed, the curves in Fig. 3(a) are calculated without additional parameters. Additional fitting parameters used to describe Fig. 3(b) are as follows: $|p'| = 700$ meV Å^2, $\phi_{p'} = \pi$, and $S' = 70$ meV Å^2.

In the high-field limit, $\chi_L \chi_R / (\chi_L^2 + \chi_R^2) \to 0$ so that either $\chi_L^2 \ll \chi_R^2$ or $\chi_L^2 \gg \chi_R^2$, and Eqs. (15) and (20) transfer to

$$\Delta_v = 2|\lambda| \max\{\chi_L^2, \chi_R^2\},$$

$$\alpha_\pm = 2\ \mathrm{sgn}\{F_z^{N+1}\}[S \pm |p| \cos(\phi_p - \phi_\lambda)] \max\{\chi_L^2, \chi_R^2\},$$

$$\beta_\pm = 2\ \mathrm{sgn}\{F_z\}[-S' \mp |p'| \cos(\phi_{p'} - \phi_\lambda)] \max\{\chi_L^2, \chi_R^2\}.$$

Since one of the interfaces becomes inaccessible to the electron, the oscillatory behavior vanishes in strong fields.

It should be stressed that the parity of the coefficients $\alpha_\pm$ and $\beta_\pm$ following from the above equations completely agrees with the general symmetry considerations, [Eqs. (2) and (3)]. We also note that a monoatomic shift as a whole of the QW position in the structure results in a sign inversion for $\alpha_\pm$ while the values of $\beta_\pm$ remain unchanged. Indeed, taking into account that in the diamondlike lattice the nearest neighbors lie in the (110) and $(1\bar{1}0)$ planes, the monoatomic shift is equivalent to a rotation of the coordinate frame around the z axis by the angle $\pi/2$. Under this transformation, the combination $h(\boldsymbol{k}) = \sigma_x k_x - \sigma_y k_y$ reverses its sign, whereas $h'(\boldsymbol{k}) = \sigma_x k_y - \sigma_y k_x$ keeps unchanged.

V. CONCLUSION

The $sp^3d^5s^*$ tight-binding model has been used to calculate the electron dispersion in heterostructures grown from multivalley semiconductors with the diamond lattice, particularly, in the Si/SiGe structures. The model allows one to quantitatively estimate the valley and spin splittings of electron states in the quantum-confined ground subband as well as the electric field dependence of the spin splitting. In the employed tight-binding model, this splitting is mostly determined by the spin-dependent mixing at the interfaces. As a result, the coefficients describing the IIA term (or the generalized Dresselhaus term) in unbiased QWs are oscillating functions of the odd number N of Si monoatomic layers. Under an electric field applied along the growth axis, a nonzero Rashba term appears in QWs with both even and odd Si-atomic layers. In small fields, the Dresselhaus term is linear in the structures with even N (D_{2h} point group) and quadratic in structures with odd N (D_{2d} point group). Thus, in quite low fields about 10^{-4} V cm, the spin splitting becomes anisotropic and oscillations as a function of the QW width are suppressed. In addition to numerical calculations, an extended envelope-function approach is utilized to interpret the results of tight-binding calculations. The inclusion of spin-dependent reflection of an electronic wave at the interface and interface-induced intervalley mixing permits one to describe quite well the numerical dependencies of the valley-orbit and spin-orbit splittings upon the number of Si-atomic planes and the electric field.

ACKNOWLEDGMENTS

This work was financially supported by RFBR and CNRS PICS projects, programs of RAS, and "Dynasty" Foundation (ICFPM).

[1] E. I. Rashba, Fiz. Tverd. Tela (Leningrad) **2**, 1224 (1960); [Sov. Phys. Solid State **2**, 1109 (1960)].

[2] Y. A. Bychkov and E. I. Rashba, Pis'ma Zh. Eksp. Teor. Fiz. **39**, 66 (1984); [JETP Lett. **39**, 78 (1984)].

[3] L. Vervoort, R. Ferreira, and P. Voisin, Phys. Rev. B **56**, R12744 (1997).

[4] L. Vervoort, R. Ferreira, and P. Voisin, Semicond. Sci. Technol. **14**, 227 (1999).

[5] E. L. Ivchenko, A. Y. Kaminski, and U. Rössler, Phys. Rev. B **54**, 5852 (1996).

[6] T. Guettler, A. L. C. Triques, L. Vervoort, R. Ferreira, P. Roussignol, P. Voisin, D. Rondi, and J. C. Harmand, Phys. Rev. B **58**,

R10179 (1998).
[7] J. T. Olesberg, W. H. Lau, M. E. Flatté, C. Yu, E. Altunkaya, E. M. Shaw, T. C. Hasenberg, and T. F. Boggess, Phys. Rev. B **64**, 201301(R) (2001).
[8] K. C. Hall, K. Gündoğdu, E. Altunkaya, W. H. Lau, M. E. Flatté, T. F. Boggess, J. J. Zinck, W. B. Barvosa-Carter, and S. L. Skeith, Phys. Rev. B **68**, 115311 (2003).
[9] L. E. Golub and E. L. Ivchenko, Phys. Rev. B **69**, 115333 (2004).
[10] T. B. Boykin, G. Klimeck, M. Friesen, S. N. Coppersmith, P. von Allmen, F. Oyafuso, and S. Lee, Phys. Rev. B **70**, 165325 (2004).
[11] M. O. Nestoklon, L. E. Golub, and E. L. Ivchenko, Phys. Rev. B **73**, 235334 (2006).
[12] J.-M. Jancu, R. Scholz, E. A. de Andrada e Silva, and G. C. La Rocca, Phys. Rev. B **72**, 193201 (2005).
[13] A. Valavanis, Z. Ikonic, and R. W. Kelsall, Phys. Rev. B **75**, 205332 (2007).
[14] M. Virgilio and G. Grosso, Phys. Rev. B **75**, 235428 (2007).
[15] M. Friesen, S. Chutia, C. Tahan, and S. N. Coppersmith, Phys. Rev. B **75**, 115318 (2007).
[16] D. Ahn, J. Appl. Phys. **98**, 033709 (2005).
[17] J.-M. Jancu, R. Scholz, F. Beltram, and F. Bassani, Phys. Rev. B **57**, 6493 (1998).
[18] J.-M. Jancu and P. Voisin, Phys. Rev. B **76**, 115202 (2007).
[19] F. Sacconi, A. Di Carlo, P. Luigli, M. Städele, and J.-M. Jancu, IEEE Trans. Electron Devices **51**, 704 (2004).
[20] G. Bir and G. Pikus, *Symmetry and Strain Induced Effects in Semiconductors* (Wiley, New York, 1974).
[21] G. Klimeck, R. C. Bowen, T. B. Boykin, C. Salazar-Lazaro, T. A. Cwik, and A. Stoica, Superlattices Microstruct. **27**, 77 (2000).
[22] J.-M. Jancu, R. Scholz, G. C. La Rocca, E. A. de Andrada e Silva, and P. Voisin, Phys. Rev. B **70**, 121306(R) (2004).
[23] J. C. Slater and G. F. Koster, Phys. Rev. **94**, 1498 (1954).
[24] P.-O. Löwdin, J. Chem. Phys. **18**, 365 (1950).
[25] S. Y. Ren, J. D. Dow, and D. J. Wolford, Phys. Rev. B **25**, 7661 (1982).
[26] C. G. Van de Walle, Phys. Rev. B **39**, 1871 (1989).
[27] P. N. Keating, Phys. Rev. **145**, 637 (1966).
[28] J. E. Bernard and A. Zunger, Phys. Rev. B **44**, 1663 (1991).
[29] M. M. Rieger and P. Vogl, Phys. Rev. B **48**, 14276 (1993).
[30] F. Schäffler, Semicond. Sci. Technol. **12**, 1515 (1997).
[31] M. Virgilio, Ph.D. thesis, Universita di Pisa, 2008.
[32] T. B. Boykin and P. Vogl, Phys. Rev. B **65**, 035202 (2001).
[33] Z. Wilamowski, W. Jantsch, H. Malissa, and U. Rössler, Phys. Rev. B **66**, 195315 (2002).
[34] M. M. Glazov, Phys. Rev. B **70**, 195314 (2004).
[35] P. Pfeffer and W. Zawadzki, Phys. Rev. B **59**, R5312 (1999).